Applied Physics Letters

RESEARCH ARTICLE | MAY 22 2023

Universal scaling of droplet retraction dynamics on vibrating surfaces

Special Collection: Superhydrophobic Surfaces

Mingkai Song ; Xiaonan Liu ; Ting Wang ; Wanghuai Xu ; Shengteng Zhao ; Shunbo Wang ; Zuankai Wang ; Hongwei Zhao

Appl. Phys. Lett. 122, 214102 (2023)
https://doi.org/10.1063/5.0152599

Applied Physics Letters ARTICLE pubs.aip.org/aip/apl

Universal scaling of droplet retraction dynamics on vibrating surfaces

Cite as: Appl. Phys. Lett. **122**, 214102 (2023); doi: 10.1063/5.0152599
Submitted: 31 March 2023 · Accepted: 17 April 2023 ·
Published Online: 22 May 2023

View Online Export Citation CrossMark

Mingkai Song,[1] Xiaonan Liu,[2] Ting Wang,[2] Wanghuai Xu,[3] Shengteng Zhao,[1] Shunbo Wang,[1] Zuankai Wang,[3,a)] and Hongwei Zhao[1,4,a)]

AFFILIATIONS

[1]School of Mechanical and Aerospace Engineering, Jilin University, Changchun 130025, People's Republic of China
[2]Department of Mechanical Engineering, City University of Hong Kong, Hong Kong 999077, People's Republic of China
[3]Department of Mechanical Engineering, The Hong Kong Polytechnic University, Hong Kong 999077, People's Republic of China
[4]Key Laboratory of CNC Equipment Reliability, Ministry of Education, Changchun 130025, People's Republic of China

Note: This paper is part of the APL Special Collection on Superhydrophobic Surfaces.
[a)]**Authors to whom correspondence should be addressed:** zk.wang@polyu.edu.hk and hwzhao@jlu.edu.cn

ABSTRACT

Over the past decade, extensive efforts have been made in the study of droplet impact, especially on stationary surfaces, owing to its direct applications in thermal cooling, self-cleaning, and power generation. However, many practical applications, such as ultrasonic cleaning, aerosolized drug delivery, and vibration-assisted welding, involve the direct interaction of droplets with vibrating surfaces, on which droplets undergo spreading and retraction. Distinct from stationary surfaces where the retraction behaviors, such as the retraction velocity and rate, are mainly governed by the surface wettability and droplet inertia, the retraction behaviors on vibrating surfaces become complicated due to the vibration velocity, which dictates the outcomes of droplet impact, such as the pinning, bouncing, gyrating, and jetting. Here, we revealed the synergistic effect of droplet inertia and vibration velocity on droplet retraction. We found that the droplet retraction behaviors on both stationary and vibrating surfaces could be characterized by a universal scaling law, allowing us to analyze and predict the maximum droplet retraction velocities. Moreover, we found that the maximum retraction rate increased with the maximum spreading radius at low Weber numbers. We demonstrated that the droplet retraction dynamics at both low Weber numbers and high Weber numbers could be unified into one integrated model, which indicates the decisive role of the maximum droplet spreading in droplet retraction dynamics.

Droplet impact on solid surfaces is common in nature and important in numerous industrial applications, such as inkjet printing,[1] thermal cooling,[2,3] self-cleaning,[4] and power generation.[5,6] Many of the droplet-impacting outcomes, such as bouncing,[7,8] jetting,[9,10] gyrating,[11] and dewetting,[12] are mediated by droplet retraction behaviors. In general, droplet retraction behaviors occur more easily on hydrophobic and especially superhydrophobic surfaces, depending on the synergy of droplet inertia, liquid viscosity, substrate macrotexture,[13,14] and surface wettability.[15] Previous studies have focused on droplet retraction behaviors with high impacting velocities on hydrophobic stationary surfaces.[16] However, practical surfaces, such as the swaying plant leaves, the flapping animal wings, and the sparking water of the lake, are always accompanied by different levels of vibration. Imposing vibration to surfaces can promote the spreading,[17] atomization,[18] directional transport,[19] and Cassie–Wenzel wetting transition[20,21] of droplets, which has widely been used in ultrasonic cleaning,[22] anti-icing of wings,[23] aerosolized drug delivery,[24,25] and vibration-assisted welding.[26] Despite extensive progress, a quantitive understanding of how vibration affects droplet retraction behaviors remains unclear. Indeed, droplet retraction behaviors on vibrating surfaces are more complex and prevalent than that on stationary surfaces, which may contribute to preventing surface icing, removing surface dust, enhancing convection heat transfer, and improving power generation efficiency (Fig. 1).

In this Letter, we aim at illustrating the effect of droplet inertia and vibration velocity on droplet retraction dynamics [Fig. 2 (Multimedia view)]. We introduced the Weber number $We = 2\rho U_i^2 R_0/\gamma$ to quantify the droplet inertia and the vibration Weber number $We^* = 2\rho U_v^2 R_0/\gamma$ to quantify the vibration velocity, where ρ, γ, U_i, U_v, and R_0 are density, surface tension coefficient, impacting velocity of droplets, velocity amplitude of vibration, and initial droplet radius, respectively. In analogy to the Weber number to characterize

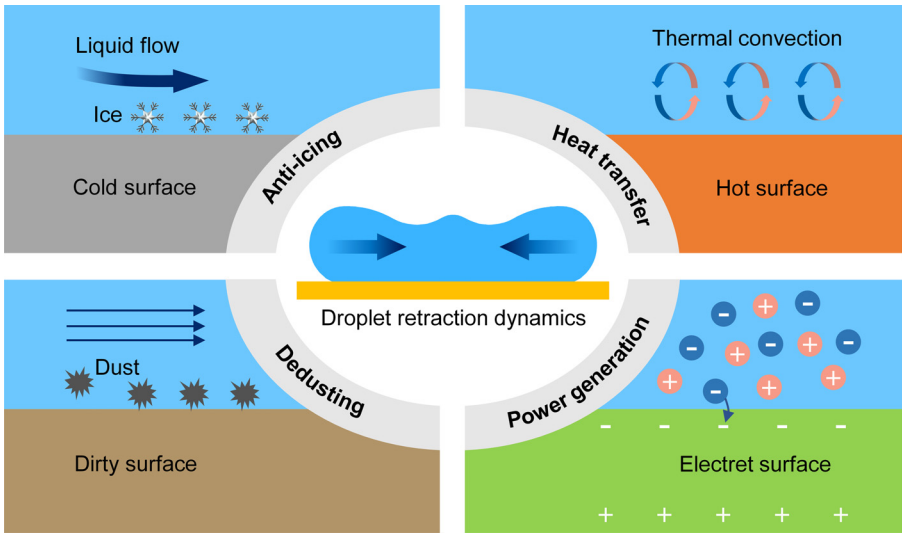

FIG. 1. Applications of droplet retraction dynamics. Imposing vibration to surfaces may help to prevent surface icing, remove surface dust, enhance convection heat transfer, and improve power generation efficiency.

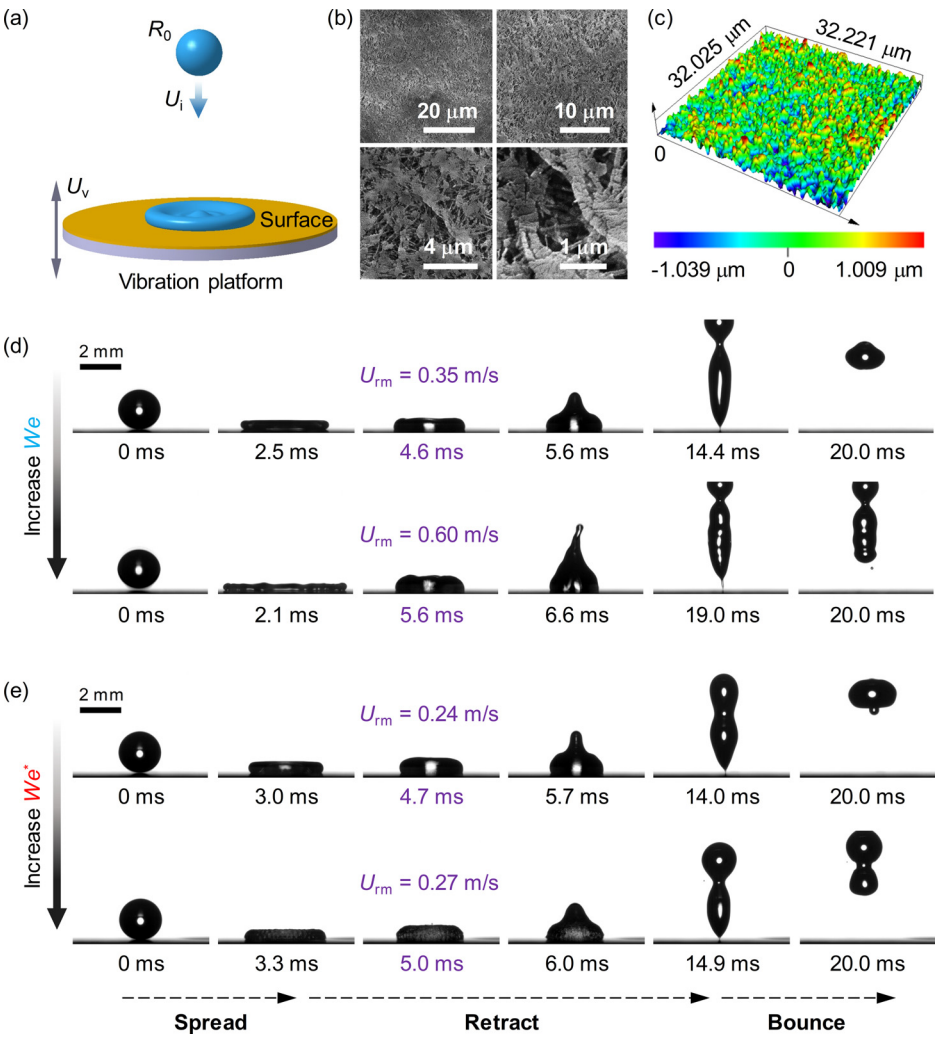

FIG. 2. Characterization of droplet retraction on flat porous polytetrafluoroethylene (PTFE) surface. (a) Experimental schematic diagram of droplet retraction on vibrating surfaces. The symbols R_0, U_i, and U_v represent the initial droplet radius, the impacting velocity, and the vibration velocity amplitude, respectively. (b) Scanning electron microscope images of the porous PTFE surface. (c) Laser confocal microscope image of the porous PTFE surface. (d) and (e) show droplet retraction on stationary surfaces and vibrating surfaces, respectively. The symbol We is the Weber number defined as $We = 2\rho U_i^2 R_0/\gamma$ and We^* is the vibration Weber number defined as $We^* = 2\rho U_v^2 R_0/\gamma$, where ρ and γ are the liquid density and surface tension coefficient, respectively. On stationary surfaces, the maximum droplet retraction velocity U_{rm} increases from 0.35 to 0.60 m/s when the Weber number We increases from 34 to 109. On vibrating surfaces, the maximum droplet retraction velocity U_{rm} increases from 0.24 to 0.27 m/s when the vibration Weber number We^* increases from 1.1 to 7.1 at $We = 16$. Multimedia available online.

the droplet dynamics on stationary surfaces, the vibration Weber number incorporates the vibration velocity to quantify the competition between the vibration-induced time-averaged dynamic pressure and surface tension.[17] Based on the Weber number and the vibration Weber number, we investigated the maximum retraction velocities on stationary and vibrating surfaces, respectively. We found that the maximum retraction velocity on both stationary surfaces and vibrating surfaces followed a universal scaling law, allowing us to quantitively analyze and predict the droplet retraction behaviors. In addition, we observed the variation of the maximum retraction rate at low Weber numbers and demonstrated that droplet retraction behaviors at low Weber numbers and high Weber numbers can be unified into one integrated model, indicating that the maximum droplet spreading was decisive for droplet retraction dynamics.

Droplet retraction dynamics on vibrating surfaces was first studied [Fig. 2(a)]. The experimental device was composed of a vibration platform and a droplet producer. The vibration platform consisted of a power supply, a piezoelectric transducer, and an amplitude transformer. The vibration platform could generate harmonic vibration with a frequency of 10 kHz in the vertical direction, and the vibration velocity could be controlled by adjusting the output voltage of the power supply. The droplet producer consisted of a syringe pump, an infusion tube, and an injection needle. The droplet producer could produce water droplets with a diameter of ~2.1 mm, and the impact velocity of the droplet could be controlled by adjusting the height of the needle from the vibrating surface. During the experiment, a flat hydrophobic porous polytetrafluoroethylene (PTFE) surface was firmly pasted on the vibration platform [Figs. 2(b) and 2(c)]. The PTFE surface had a thickness of ~20 μm, a contact angle of $\theta = 140 \pm 3°$, an advancing angle of $\theta_a = 160 \pm 4°$, and a receding angle of $\theta_r = 124 \pm 2°$. The PTFE surface was forced to vibrate harmoniously with the vibration platform. To avoid atomization of droplets on the vibrating PTFE surface, the velocity amplitude of the PTFE surface was controlled below the value of 0.5 m/s.

The droplet retraction behaviors were observed through a high-speed motion analysis system, which included a white light source, a set of lenses, and a high-speed camera (Phantom VEO 410L-18G). The sample rate of the camera was set to 10 000 frames per second (fps). The resolution of the camera was set to 1024×512 pixels^2, and the exposure time of the camera was set to 99 μs. Moreover, the vibration velocity of the PTFE surface was measured in real time by a Doppler laser vibrometer [LV-FS01, Sunny Optical Technology (Group) Company Limited]. The laser wavelength of the vibrometer was 1550 nm. The sampling frequency of the vibrometer was set to 960 000 Hz. The analysis frequency of the vibrometer was set to 375 000 Hz. After the experiment, the droplet velocities and sizes were extracted from the camera videos. All experiments were carried out under normal laboratory conditions at 25 °C.

Droplet retraction behaviors on vibrating surfaces are similar to that on stationary surfaces, but the retraction velocity varies with the droplet inertia and the vibration velocity [Figs. 2(d) and 2(e)]. We found that the maximum retraction velocity of the droplet, U_{rm}, varied with the Weber number We and the vibration Weber number We^*. On stationary surfaces, the maximum retraction velocity U_{rm} increases from 0.35 to 0.60 m/s when the Weber number We increases from 34 to 109 [Fig. 2(d)]. On vibrating surfaces, the maximum retraction velocity U_{rm} increases from 0.24 to 0.27 m/s when the vibration Weber number We^* increases from 1.1 to 7.1 at $We = 16$ [Fig. 2(e)]. In particular, we found that the retraction radius of droplets at the maximum retraction velocity on stationary surfaces was close to that on vibrating surfaces, but the maximum spreading radius of droplets varied with the Weber number and the vibration Weber number, which caused the variation of the retraction velocity [Figs. 2(d) and 2(e)].

To determine the relationship between the droplet retraction velocity and the spreading/retraction radius, we first investigated the evolution of the spreading and retraction radius with time. The radius $R(t)$ increases first and then decreases on both stationary surfaces and vibrating surfaces, leading to a maximum spreading radius R_m at a certain moment t_m [Figs. 3(a) and 3(b)]. The maximum spreading radius R_m varies with the Weber number We and the vibration Weber number We^*. If we transform the vertical coordinates $R(t)$ and the horizontal coordinates t in Figs. 3(a) and 3(b) into $[R_m - R(t)]$ and $(t - t_m)$, respectively, then the slope of the curves represents the retraction velocity of droplets [see Figs. 3(c) and 3(d)]. For example, the maximum slope of the curve with $We = 109$ is larger than that with $We = 34$, indicating that the maximum retraction velocity U_{rm} at $We = 109$ is larger than that at $We = 34$ [see Fig. 3(c)]. We further investigated the maximum retraction velocities of droplets at different Weber numbers and vibration Weber numbers extensively. We found that the maximum retraction velocity U_{rm} increased with the Weber number We and the vibration Weber number We^*. For example, at $We^* = 7.1$, the maximum droplet retraction velocity U_{rm} increases from ~0.11 to ~0.60 m/s when We increases from 8 to 109 [Fig. 3(e)]. However, at $We = 34$, the maximum droplet retraction velocity U_{rm} only increases from ~0.32 to ~0.37 m/s when We^* increases from 0 to 7.1 [Fig. 3(f)]. Compared with We^*, the Weber number We was more effective in droplet retraction. In reality, the Weber number dominated the droplet retraction dynamics at $We^* < 10 < We$ [Figs. 3(e) and 3(f)].

In the following, we considered the energy conversion of droplets during the retraction. From the "maximum spreading" to the "maximum retraction velocity" of droplets, the reduced surface energy of the droplet film was converted into the translational kinetic energy and the internal energy of the droplet rim, ignoring the effects of gravity and vibration-induced pressure [Fig. 4(a)]. The reduced surface energy is $\Delta E_s \sim \pi\gamma(1 - \cos\theta_r)(R_m^2 - R_r^2)$, where R_r is the retraction radius of the droplet at the maximum retraction velocity. The increased kinetic energy and internal energy are, respectively, $\Delta E_k \sim \frac{1}{2}(\frac{4}{3}\pi\rho R_0^3)U_{rm}^2$ and $\Delta E_i \sim \frac{1}{2}(\pi\rho h R_m^2)U_{rm}^2$, where h is the thickness of the droplet film.[27] Based on the law of conservation of energy, we obtain the following equation:

$$\Delta E_s = \Delta E_k + \Delta E_i. \tag{1}$$

Compared with ΔE_k, the energy ΔE_i is small enough to be ignored, leading to $\Delta E_s \sim \Delta E_k$. Substitute the maximum spreading factor $\beta_m = R_m/R_0$ and the retraction factor $\beta_r = R_r/R_0$ into Eq. (1), then we can get the following power-law relation:

$$U_{rm}^2 \sim \frac{3\gamma}{2\rho R_0}(1 - \cos\theta_r)(\beta_m^2 - \beta_r^2). \tag{2}$$

The maximum retraction velocity U_{rm} increases with $(\beta_m^2 - \beta_r^2)^{1/2}$, indicating the dependence of droplet retraction on droplet spreading. We have plotted U_{rm} as a function of $(\beta_m^2 - \beta_r^2)$ in the logarithmic

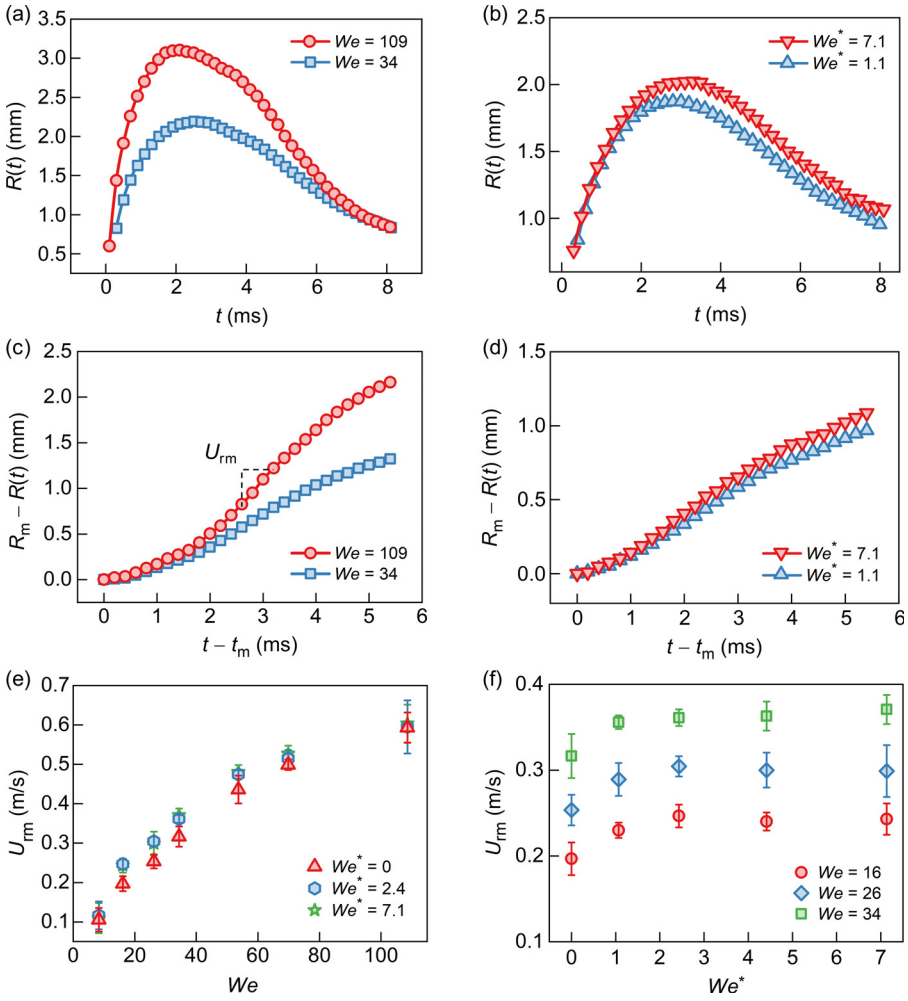

FIG. 3. Evolution of the droplet spreading and retraction radius with time. (a) and (b) show the time-dependent radius $R(t)$ vs time t on stationary surfaces and vibrating surfaces, respectively. (c) and (d) are plotted by transforming the coordinates $R(t)$ and t in (a) and (b) into $[R_m - R(t)]$ and $(t - t_m)$, respectively. The symbol R_m is the maximum spreading radius, and t_m is the time corresponding to R_m. The slope of the curves in (c) and (d) represents the retraction velocity of droplets. (e) and (f) show the maximum retraction velocities of droplets at different Weber numbers and vibration Weber numbers. Data are mean ± s.d. except when indicated ($n = 3$).

coordinate diagram [Fig. 4(b)]. All the data are collapsed into the fitting line with a slope of 0.5, faithfully following Eq. (2) with a numerical coefficient of 0.6. We investigated the variation of β_m and β_r under different conditions. On stationary surfaces, the maximum spreading factor β_m is determined by the scaling law, $\beta_m \propto We^{1/4}$, with a numerical coefficient of 0.88 [Fig. 4(c)].[28] On vibrating surfaces, the maximum spreading factor β_m is determined by the scaling law, $(\beta_m/\beta_{m0} - 1) \propto We^*/[We^{1/2}\sin(\theta/2)]$, with a numerical coefficient of 0.051, where β_{m0} is the maximum spreading factor at $We^* = 0$ [Fig. 4(d)].[17] In contrast to β_m, the retraction factor β_r is independent of We and We^* at high Weber numbers. Specifically, the retraction factor β_r is close to a material constant of 1.64 at $We > 20$, which implies that the profiles of droplets at the maximum retraction velocity have a geometric similarity [see Figs. 2(d), 2(e), and 4(e)].

In contrast to the maximum retraction velocity U_{rm}, the maximum retraction rate of droplets, $\dot{\varepsilon} = U_{rm}/R_m$, is generally considered to be independent of We at high Weber numbers.[16] However, the scaling relation between $\dot{\varepsilon}$ and We is more complex at low Weber numbers.[29] In this study, we analyzed the factors that affect the maximum retraction rate of droplets at low Weber numbers. By substituting $U_{rm} = \dot{\varepsilon} R_m$ into Eq. (2), we get the scaling relation between $\dot{\varepsilon}$ and β_m,

$$\frac{U_{rm}}{R_m} = \tau_i^{-1}\sqrt{a_1\pi(1-\cos\theta_r) - a_2\beta_m^{-2}}, \tag{3}$$

where a_1 and a_2 are positive coefficients associated with the surface properties, and τ_i is the inertial timescale of the droplet expressed as $\tau_i = (\frac{4}{3}\pi\rho R_0^3/\gamma)^{1/2}$. Equation (3) indicates that the maximum retraction rate $\dot{\varepsilon}$ increases with the maximum spreading factor β_m at low Weber numbers [Fig. 4(f)]. Meanwhile, Eq. (3) predicts that $\dot{\varepsilon}$ will approach a material constant, $\tau_i^{-1}\sqrt{a_1\pi(1-\cos\theta_r)}$, independent of We at $\beta_m^{-2} \to 0$, which has been confirmed by the experimental results of droplet retraction at high Weber numbers.[16] We have used Eq. (3) to fit the data in Fig. 4(f). The data are collapsed into the fitted curve with $a_1 \approx 0.52$ and $a_2 \approx 5.4$.

In this study, we analyzed the effect of droplet inertia and vibration velocity on the maximum retraction velocity and maximum retraction rate of droplets. Our analysis indicates that both U_{rm} and U_{rm}/R_m increase with the maximum spreading factor β_m and, thus, with the Weber number We and the vibration Weber number We^* [see Eqs. (2) and (3)]. Here, we must stress that the analysis is for low-viscous droplets based on the condition of $We \gg 1$ and $We^* < 10$. For $We \sim 1$ and $We < 1$, Eqs. (1)–(3) may be inapplicable because the

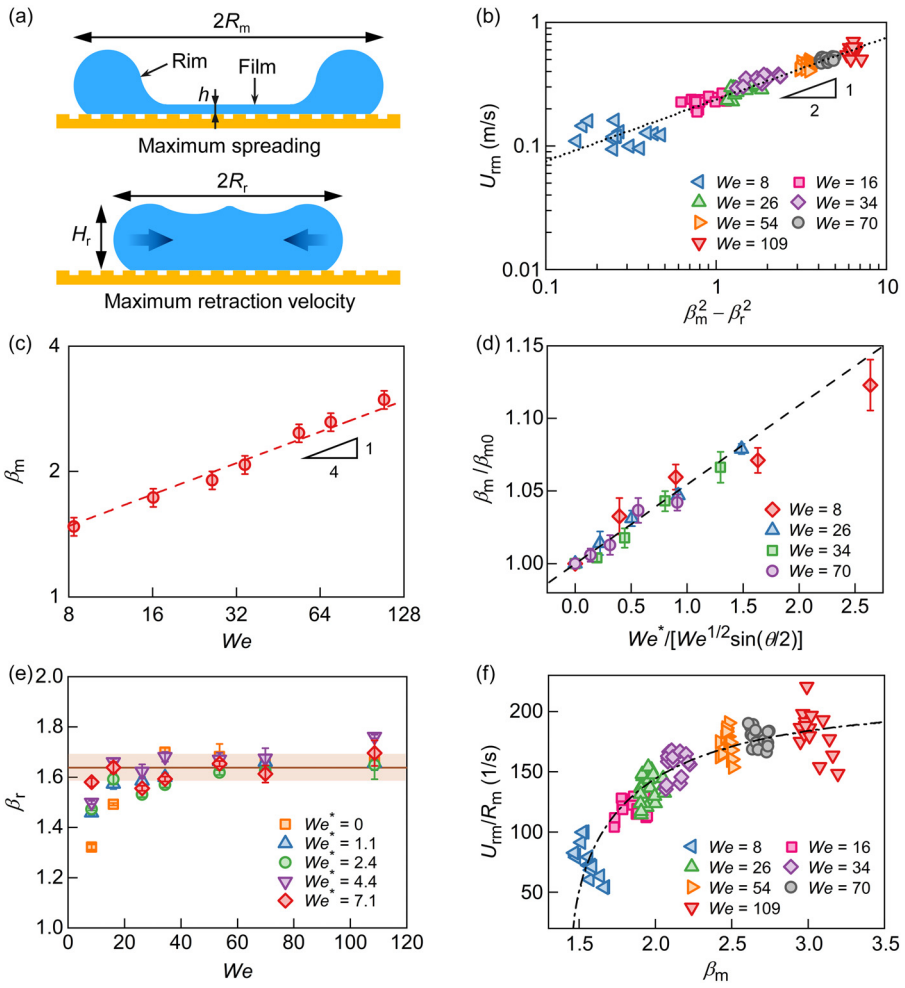

FIG. 4. Scaling relation between droplet spreading and retraction. (a) The symbol h is the thickness of the droplet film. The symbols R_r and H_r are the droplet retraction radius and height, respectively. (b) Power law relationship between U_{rm} and $(\beta_m^2 - \beta_r^2)$, where β_m is the maximum spreading factor defined as $\beta_m = R_m/R_0$ and β_r is the retraction factor defined as $\beta_r = R_r/R_0$. (c) and (d) show the scaling law of droplet spreading on stationary surfaces and vibrating surfaces, respectively. The symbol β_{m0} is the maximum spreading factor at $We^* = 0$ and θ is the contact angle. (e) Variation of β_r with the Weber number We. (f) shows the dependence of U_{rm}/R_m on β_m. Error bars in (c)–(e), ±1 s.d. with $n = 3$ each. The dotted line in (b) is the fitted curve using the form of Eq. (2). Dashed lines in (c) and (d) are fitted curves using the form of $\beta_m \propto We^{1/4}$ and $(\beta_m/\beta_{m0} - 1) \propto We^*/[We^{1/2}\sin(\theta/2)]$, respectively. The solid line in (e) is the averaged β_r calculated by the data of $We > 20$. The dashed–dotted line in (f) is the fitted curve using the form of Eq. (3).

droplets are difficult to fully spread to form the rim and the film (Supplementary material Fig. S1). For $We^* \gg 10$, the droplets become unstable on vibrating surfaces and are easy to be atomized (Supplementary material Fig. S2). Moreover, our analysis is based on droplet retraction dynamics on flat smooth hydrophobic/superhydrophobic surfaces without macrotexture, which is not applied to hydrophilic surfaces (Supplementary material Fig. S3). In the analysis, we did not consider the effect of the substrate deformation,[30] surface microtexture,[31] and droplet shape[32] on the droplet retraction dynamics, which may cause the deviation of the experimental data. Nonetheless, our study revealed the scaling law between droplet spreading and retraction, allowing us to analyze and predict the maximum retraction velocity and rate of droplets, which may help to understand and control other droplet behaviors.

In summary, we studied droplet retraction behaviors on stationary surfaces and vibrating surfaces, respectively. We found that the maximum retraction velocity of droplets increased with the Weber number We and the vibration Weber number We^*. Based on the conservation of energy, we proposed a simple but effective formula to analyze the droplet retraction velocities and demonstrated that the maximum retraction velocity of droplets on both stationary surfaces and vibrating surfaces could be predicted by the universal scaling law, $U_{rm}^2 \sim \frac{3\gamma}{2\rho R_0}(1 - \cos\theta_r)(\beta_m^2 - \beta_r^2)$. The maximum spreading factor β_m was observed to increase with the Weber number We and the vibration Weber number We^*. In contrast to β_m, the retraction factor β_r was observed close to a material constant independent of We and We^* at high Weber numbers, indicating the similarity of fluid flow during the droplet retraction. Moreover, we unified the droplet retraction dynamics at low Weber numbers and high Weber numbers into one integrated model and clarified the dependence of the maximum retraction rate U_{rm}/R_m on the maximum spreading factor β_m [see Eq. (3)]. We hope that our findings of the scaling relation between droplet spreading and retraction dynamics would be helpful for industrial applications, such as anti-icing, dedusting, and heat transfer.

See the supplementary material for more videos of droplet dynamics and details of experiments and analysis.

We acknowledge the financial support from the National Natural Science Foundation of China (No. 51975502), the

Foundation for Innovative Research Groups of the National Natural Science Foundation of China (No. 52021003), the Research Grants Council of Hong Kong (Nos. SRFS2223-1S01, C1006-20W, 11213320, and 11219219), the Shenzhen Science and Technology Innovation Council (No. SGDX20201103093005028), the National Natural Science Foundation of Jilin Province (No. 20200201231JC), the Scientific Research Project of Jilin Provincial Department of Education (No. JJKH20220982KJ), and the Innovation and Technology Commission of Hong Kong (Nos. GHP/021/19SZ and GHP/092/20GD).

AUTHOR DECLARATIONS

Conflict of Interest

The authors have no conflicts to disclose.

Author Contributions

Mingkai Song: Investigation (equal); Methodology (equal); Writing – review & editing (equal). **Xiaonan Liu:** Writing – review & editing (equal). **Ting Wang:** Writing – review & editing (equal). **Wanghuai Xu:** Writing – review & editing (equal). **Shengteng Zhao:** Investigation (equal); Methodology (equal). **Shunbo Wang:** Investigation (equal); Methodology (equal). **Zuankai Wang:** Resources (equal); Writing – review & editing (equal). **Hongwei Zhao:** Resources (equal); Writing – review & editing (equal).

DATA AVAILABILITY

The data that support the findings of this study are available within the article and the supplementary material.

REFERENCES

[1]D. Lohse, Annu. Rev. Fluid Mech. **54**, 349 (2022).
[2]M. Jiang, Y. Wang, F. Liu, H. Du, Y. Li, H. Zhang, S. To, S. Wang, C. Pan, J. Yu, D. Quéré, and Z. Wang, Nature **601**, 568 (2022).
[3]X. Zhao, Z. Yin, B. Zhang, and Z. Yang, Int. J. Heat Mass Transfer **146**, 118819 (2020).
[4]F. Geyer, M. D'Acunzi, A. Sharifi-Aghili, A. Saal, N. Gao, A. Kaltbeitzel, T.-F. Sloot, R. Berger, H.-J. Butt, and D. Vollmer, Sci. Adv. **6**, eaaw9727 (2020).
[5]N. Zhang, H. Zhang, W. Xu, H. Gu, S. Ye, H. Zheng, Y. Song, Z. Wang, and X. Zhou, Droplet **1**, 56 (2022).
[6]W. Xu, H. Zheng, Y. Liu, X. Zhou, C. Zhang, Y. Song, X. Deng, M. Leung, Z. Yang, R. X. Xu, Z. L. Wang, X. C. Zeng, and Z. Wang, Nature **578**, 392 (2020).
[7]X. Yu, Y. Zhang, R. Hu, and X. Luo, Nano Energy **81**, 105647 (2021).
[8]Y. Liu, L. Moevius, X. Xu, T. Qian, J. M. Yeomans, and Z. Wang, Nat. Phys. **10**, 515 (2014).
[9]D. Bartolo, C. Josserand, and D. Bonn, Phys. Rev. Lett. **96**, 124501 (2006).
[10]K. Yamamoto, M. Motosuke, and S. Ogata, Appl. Phys. Lett. **112**, 093701 (2018).
[11]H. Li, W. Fang, Y. Li, Q. Yang, M. Li, Q. Li, X.-Q. Feng, and Y. Song, Nat. Commun. **10**, 950 (2019).
[12]A. M. J. Edwards, R. Ledesma-Aguilar, M. I. Newton, C. V. Brown, and G. McHale, Sci. Adv. **2**, e1600183 (2016).
[13]A. Gauthier, S. Symon, C. Clanet, and D. Quéré, Nat. Commun. **6**, 8001 (2015).
[14]Y. Liu, M. Andrew, J. Li, J. M. Yeomans, and Z. Wang, Nat. Commun. **6**, 10034 (2015).
[15]S. Hu, X. Cao, T. Reddyhoff, X. Ding, X. Shi, D. Dini, A. J. deMello, Z. Peng, and Z. Wang, Droplet **1**, 48 (2022).
[16]D. Bartolo, C. Josserand, and D. Bonn, J. Fluid Mech. **545**, 329 (2005).
[17]M. Song, H. Zhao, T. Wang, S. Wang, J. Wan, X. Qin, and Z. Wang, J. Colloid Interface Sci. **608**, 2414 (2022).
[18]K. Yoshioka, Y. Kurashina, A. Ogawa, and T. Asakura, Ultrason. Sonochem. **86**, 106019 (2022).
[19]D. Wu, Z. Zhang, Y. Zhang, Y. Jiao, S. Jiang, H. Wu, C. Li, C. Zhang, J. Li, Y. Hu, G. Li, J. Chu, and L. Jiang, Adv. Mater. **32**, e2005039 (2020).
[20]A. Sudeepthi, L. Yeo, and A. K. Sen, Appl. Phys. Lett. **116**, 093704 (2020).
[21]W. Lei, Z.-H. Jia, J.-C. He, T.-M. Cai, and G. Wang, Appl. Phys. Lett. **104**, 181601 (2014).
[22]S. Aghapour Aktij, A. Taghipour, A. Rahimpour, A. Mollahosseini, and A. Tiraferri, Ultrasonics **108**, 106228 (2020).
[23]A. Khadak, B. Subeshan, and R. Asmatulu, J. Mater. Sci. **56**, 3078 (2021).
[24]M. Bok, Z.-J. Zhao, S. Jeon, J.-H. Jeong, and E. Lim, Sci. Rep. **10**, 2027 (2020).
[25]J. S. Lass, A. Sant, and M. Knoch, Expert Opin. Drug Deliv. **3**, 693 (2006).
[26]M. J. Jose, S. S. Kumar, and A. Sharma, Sci. Technol. Weld. Joining **21**, 243 (2016).
[27]F. E. C. Culick, J. Appl. Phys. **31**, 1128 (1960).
[28]C. Clanet, C. Béguin, D. Richard, and D. Quéré, J. Fluid Mech. **517**, 199 (2004).
[29]X. Deng, F. Schellenberger, P. Papadopoulos, D. Vollmer, and H.-J. Butt, Langmuir **29**, 7847 (2013).
[30]J. Gerber, T. Lendenmann, H. Eghlidi, T. M. Schutzius, and D. Poulikakos, Nat. Commun. **10**, 4776 (2019).
[31]T. Mouterde, P. Lecointre, G. Lehoucq, A. Checco, C. Clanet, and D. Quéré, Nat. Commun. **10**, 1410 (2019).
[32]Q. Liu, J. H. Y. Lo, Y. Li, Y. Liu, J. Zhao, and L. Xu, Nat. Commun. **12**, 3068 (2021).